Role of Ca^{2+} in the Electrostatic Stability and the Functional Activity of the Globular Domain of Human C1q[†]

Lubka T. Roumenina,[‡] Alexandar A. Kantardjiev,[§] Boris P. Atanasov,*,[§] Patrick Waters,[||] Mihaela Gadjeva,[⊥] Kenneth B. M. Reid,[#] Alberto Mantovani,[#,¶] Uday Kishore,*,[||,£] and Mihaela S. Kojouharova[‡]

Department of Biochemistry, Sofia University, St. Kliment Ohridski, 8 Dragan Tsankov Street, Sofia 1164, Bulgaria, and Biophysical Chemistry Laboratory, Institute of Organic Chemistry, Bulgarian Academy of Sciences, Acad. G. Bonchev Street, Sofia 1113, Bulgaria, and Weatherall Institute of Molecular Medicine, University of Oxford, John Radcliffe Hospital, Headington, Oxford OX3 9DS, United Kingdom, and Department of Pathology, Brigham and Women's Hospital, Boston, Massachusetts 02115, and MRC Immunochemistry Unit, University of Oxford, South Parks Road, Oxford, United Kingdom, and Instituto Clinico Humanitas, Rozzano Milan and Institute of General Pathology, Faculty of Medicine, University of Milan, Italy, and Institute of Medical Microbiology, Faculty of Medicine, Justus-Liebig-University, Frankfurter Strasse 107, 35392 Giessen, Germany

Received June 21, 2005; Revised Manuscript Received September 1, 2005

ABSTRACT: C1q is the recognition subunit of the classical pathway of the complement system and a major connecting link between classical pathway-driven innate immunity and IgG- or IgM-mediated acquired immunity. The basic structural subunit of C1q is composed of an N-terminal triple-helical collagen-like region and a C-terminal heterotrimeric globular head domain (gC1q) that is made up of individual A, B, and C chains. Recent crystallographic studies have revealed that the gC1q domain, which is the main target-binding region of C1q, has a compact and spherical heterotrimeric assembly, held together by both electrostatic and nonpolar interactions, with quasi-3-fold symmetry. A characteristic feature of the gC1q domain is the presence of a exposed Ca^{2+} located near the apex. We have investigated, using theoretical and experimental approaches, the role of Ca^{2+} in the electrostatic stability and target-binding properties of the native C1q as well as recombinant monomeric forms of the C-terminal regions of the A, B, and C chains. Here, we report that Ca^{2+} primarily influences the target recognition properties of C1q toward IgG, IgM, C-reactive protein, and pentraxin 3. At pH 7.4, the loss of Ca^{2+} leads to changes in the direction of electric moment from coaxial (where the putative C-reactive protein-binding site is located) to perpendicular to the molecular axis (toward the most likely IgG-binding site), which appears important for target recognition by C1q and subsequent complement activation.

C1q is the recognition subunit of the classical complement pathway and a major connecting link between classical pathway-driven innate immunity and IgG- or IgM-mediated acquired immunity (*1*). C1q is a hexameric molecule that appears as a bouquet-of-tulips-like structure under electron microscopy (*2*). It is composed of 18 polypeptide chains (6A, 6B, and 6C), and the N-terminal parts of these chains associate to yield the triple-helical collagen-like region (CLR),[1] whereas the C-terminal portion of the A, B, and C chains each contribute to the formation of the heterotrimeric globular domain (gC1q domain). The gC1q domain can recognize a broad range of target molecules, including IgG, IgM, envelope proteins of certain retroviruses, β-amyloid fibrils, lipopolysaccharides, porins from Gram-negative bacteria, phospholipids, apoptotic cells, and acute phase reactants such as C-reactive protein (CRP) and pentraxin 3 (PTX3) (*1*). Binding of the gC1q domain to these complement activators is considered to induce a conformational change in the CLR, which leads to the auto-activation of the C1q-associated serine protease proenzymes, C1r followed by C1s, and initiation of the classical complement pathway (*3, 4*).

* To whom correspondence should be addressed. Weatherall Institute of Molecular Medicine, University of Oxford, John Radcliffe Hospital, Headington, Oxford OX3 9DS, U.K. Telephone: +44-1865-222325 and +44-1865-222326. Fax: +44-1865-222402 and +49-6419-941259. E-mail: ukishore@hotmail.com (U.K.); Telephone: +359-2-9606-123. Fax: +359-2-8700-225. E-mail: boris@orgchim.bas.bg (B.P.A.).

[‡] Sofia University.
[§] Bulgarian Academy of Sciences.
[||] Weatherall Institute of Molecular Medicine, University of Oxford.
[⊥] Brigham and Women's Hospital.
[#] MRC Immunochemistry Unit, University of Oxford.
[¶] University of Milan.
[£] Justus-Liebig-University.

[1] Abbreviations: 3D EP, three-dimensional electrostatic potential; AP, alkaline phosphatase; CRP, C-reactive protein; gC1q, globular domain of C1q; CLR, collagen-like region of C1q; ghA, ghB, ghC, the recombinant forms of the carboxyl-terminal, globular region of human C1q A, B, and C chains, respectively; ACRP30, adipocyte-specific complement-related protein of 30 kDa; HRP, horseradish peroxidase; MBP, maltose-binding protein; pI, isoelectric point; PTX3, long prototypic pentraxin; TTBS, Tris-buffered saline, containing 0.05% (v/v) Tween 20.

The crystal structure of the gC1q domain of human C1q, solved at 1.9 Å resolution, has revealed its compact and spherical heterotrimeric organization, which is composed of globular regions of the A (ghA), B (ghB), and C (ghC) chains that are held together by nonpolar interactions and exhibit quasi-3-fold symmetry (*5*). Each of the individual globular head regions have a jellyroll topology consisting of a 10-stranded β sandwich made up of two 5-stranded antiparallel β sheets (*6*). This topology is a characteristic feature of members of a newly designated C1q and tumor necrosis factor (TNF) superfamily (*2, 7*).

The gC1q domain structure has also revealed the presence of a exposed Ca^{2+} ion located near the apex of the gC1q domain, at the top of a central solvent channel. The presence of Ca^{2+} has also been reported for other members of the C1q family, including collagen X (*8*) and adipocyte-specific complement-related protein of 30 kDa (ACRP30) (*11*; ACRP30 calcium complex, PDB 1C3H), both being homotrimeric structures. Neither of these proteins belong to the well-characterized calcium-binding protein families (*9*). C1q has a Ca^{2+} ion exposed to the solvent, whereas collagen X has a buried cluster of four Ca^{2+} ions, which makes an intricate network of ionic bonds that probably contribute to the high stability of its NC1 or gC1q trimer (*8*). This Ca^{2+} cluster is absent from the collagen VIII structure, a close homologue of collagen X (*10*). ACRP30 has three Ca^{2+} ions near the top of its central channel. The calcium-bound form is less disordered than the one without Ca^{2+} (*11*), providing support for a stabilizing effect of Ca^{2+}.

The Ca^{2+} ion in the gC1q structure is coordinated by six oxygen atoms: one of the side-chain oxygens of Asp^{B172}, the side-chain carbonyls of Gln^{A177} and Gln^{B179}, the main-chain carbonyl of Tyr^{B173}, and two water molecules, with an average bond length of 2.58 Å. The Ca^{2+}-binding site is therefore asymmetrical relative to the trimer. The presence of Ca^{2+} is usually related to the structural stability of the molecule, as reported for collagen X (*8*). However, data substantiating the role of Ca^{2+} in the stabilization of the gC1q domain of C1q that can alter its functional activities are not available. It has been shown that the interaction between C1q and gp41, an envelope glycoprotein of HIV-1, is Ca^{2+}-sensitive. An addition of 5 mM $CaCl_2$ has been shown to enhance binding of C1q to immune complexes by 15% (*12*). In contrast, an addition of either $CaCl_2$ or EDTA has no effect on the C1q—fibromodulin interaction (*13*).

In the present study, we sought to investigate, via theoretical and experimental approaches, the role of Ca^{2+} in the electrostatic stability and target-binding activity of the gC1q domain as well as the individual globular head fragments of human C1q (ghA, ghB, and ghC). Our results suggest that Ca^{2+} primarily influences the recognition properties of C1q toward target molecules (e.g., IgG1, IgM, CRP, and PTX3). The theoretical calculations appear to suggest that the loss of Ca^{2+} leads to changes in the direction of electric moment at pH 7.4 from coaxial to perpendicular to the molecular axis, which alters target recognition by C1q and subsequent activation of the classical complement pathway.

MATERIALS AND METHODS

Purified Proteins and Antibody Conjugates. C1q was purified from pooled human serum by affinity chromatog-raphy on IgG-Sepharose (*14*). The purity of C1q was assessed by SDS—PAGE (15%, w/v) under reducing conditions, where it appeared as three bands of 34, 32, and 27 kDa, corresponding to the A, B, and C chains, respectively. Polyclonal IgM was isolated from human plasma using gel-filtration chromatography. Monoclonal IgG1 was obtained from Mabtera and F. Hoffmann—La Roche. CRP, goat anti-rabbit IgG-alkaline phosphatase (AP) conjugate, mouse anti-MBP antibodies, and *p*-nitrophenyl phosphate (pNPP) were purchased from Sigma—Aldrich. Rabbit anti-human C1q antibodies were purchased from DAKO. Recombinant human PTX3 was expressed in Chinese hamster ovary cells and purified, as described previously (*39*).

Intracellular Expression and Purification of ghA, ghB, and ghC Modules. The recombinant globular head regions of the A chain (ghA, residues 88—223), the B chain (ghB, 90—226), and the C chain (ghC, 87—217) were expressed as fusion proteins linked to the maltose-binding protein (MBP) in *Escherichia coli* BL21 and purified, as described previously (*15*). The amount of calcium present in each recombinant module solution was assessed by atomic absorption spectroscopy using Perkin—Elmer Life Sciences, Shelton, CT equipment.

ELISA for Detecting the Interaction of C1q or Its Recombinant Fragments (ghA, ghB, and ghC) with Target Proteins (IgG1, IgM, PTX3, or CRP). Microtiter wells were coated for 1 h at 37 °C with either 2 μg/well of polyclonal IgM, 2 μg/well monoclonal IgG1, 1 μg/well human CRP, or 1μg/well recombinant human PTX3 in carbonate buffer at pH 9.6. Any nonspecific binding sites were blocked using 200 μL/well 1% (w/v) BSA for 1 h at 37 °C. The wells were then washed with PBS containing 0.05% Tween-20 and incubated with a serial dilution of C1q or recombinant forms of ghA, ghB, or ghC (from 4 to 0.03 μg/well). The incubation was carried out in Tris-buffered saline (TBS), containing 0.05% (v/v) Tween-20 (TTBS) (control experiment) and TBS either with 5 mM Ca^{2+} (for an excess of Ca^{2+}) or 20 mM EDTA overnight at 4 °C. After washing, the microtiter wells were incubated with rabbit anti-human C1q polyclonal antibodies (1:1000 dilution) or mouse anti-MBP antibodies (1:4000 dilution) for 1 h at 37 °C. Bound C1q, ghA, ghB, or ghC were detected using AP-conjugated goat anti-rabbit IgG antibodies (1:5000 dilution) or HRP-conjugated rabbit anti-mouse IgG (1:1000 dilution). pNPP or *o*-phenylenedi-amine dihydrochloride (OPD) were used as substrates for AP and HRP conjugates, respectively. The data are given as an average of three experiments ± standard deviation (SD). The plateau values using TBS were considered as 100%, and those with EDTA were used to calculate the percent reduction in C1q binding to the target.

ELISA for Detecting the Interactions of C1q, ghA, ghB, or ghC with IgG1, IgM, CRP, or PTX3 under Different pH Conditions. Incubation of immobilized targets IgG1, IgM, CRP, or PTX3 with C1q or the recombinant globular fragments (with or without Ca^{2+}) was carried out in the pH range between 3 and 8.5 in citrate—phosphate buffer [50 mM sodium citrate, 50 mM Na_2HPO_4, 140 mM NaCl, and 0.05% (v/v) Tween-20] or in the pH range between 8.5 and 12 in carbonate buffer [50 mM $NaHCO_3$, 50 mM Na_2CO_3, 140 mM NaCl, and 0.05% (v/v) Tween-20]. The amount of bound protein was detected by ELISA, as described above. The results for the pH dependence of the target binding were

presented in arbitrary units, where the minimal observed binding of C1q was taken as 0 and the maximal was taken as 1. The pH dependence of C1q binding was analyzed by fitting the data plots with the closest sigmoid curve, using the data analysis software Microcal Origin 6.0. The inflection points, representing the effective pK_a and the sharpness of the fit (the number of protons released or taken up in the process) were calculated using the equation $\Delta n_{H^+} = \partial \log(Y/1 - Y)/\partial pH$, where Y is the normalized value of target binding $(0 < Y < 1)$.

Structures. For the electrostatic calculations, the X-ray crystal structure of the gC1q domain of C1q (PDB 1PK6), which contains a Ca^{2+} ion at the apex, was used as the holo form (5). The same protein, with the Ca^{2+} ion deleted was considered to be the apo or Ca^{2+}-free form. To create the isolated A chain with the Ca^{2+} in the correct relative position, the three chains of PDB 1PK6 were separated, the B and C chains were deleted, but the Ca^{2+} was retained in its position. This was used for the calculations on the holo A chain. When the Ca^{2+} was removed, the apo form was obtained. A similar method was used to create the single B and C chains with and without the Ca^{2+} ions. The chain pairs (i.e., AB, BC, and AC) were obtained by deleting one of the three chains (the holo chain pair) or one chain and the Ca^{2+} ion (the apo chain pair).

Calculation of the Electrostatic Interactions. The electrostatic interactions of gC1q-related structures such as the ABC heterotrimer, the chain pairs (AB, AC, and BC), and the A, B, and C monomers in Ca^{2+}-bound (holo) and Ca^{2+}-free (apo) forms were calculated via (a) a mean force approach (16−19) using the program package PHEI4WIN version 5.01 (PHEI), which is extended in the PERL (A. A. Kantardjiev and B. P. Atanasov, unpublished results) and (b) a finite difference approach via a "DELPHI-SOLVER" for LINUX (20, 21). Both approaches were applied for comparison and validation of the results at preselected conditions (fixed pH, Ca^{2+} concentration, and grid focusing). Most calculations were performed using PHEI, allowing prediction of a number of pH-dependent properties based on the knowledge of pH-dependent electrostatic potential (EP) at any ith point of the system [$\Phi_{el,i}$ (pH)]. For this purpose, two sets of charges, permanent (fixed partial charges as in AMBER) (22) and titrable (proton populations, degree of ionization, and pH dependence) were used. The atomic model of C1q (PDB 1PK6) was used for all calculations (5, 23).

The pH dependence of the EP $\Phi_{el,i}$ (pH) at the ith proton-binding site in PHEI was evaluated according to eq 1.

$$\Phi_{el,i}\,(\text{pH}) = 2.3RT\sum_{j\neq i}Q_j(\text{pH})W_{ij}(1 - SA_{ij}) \quad (1)$$

Q_j(pH) represents the pH-dependent charge of a given ionic group, defined by $\langle s_j \rangle$, the degree of dissociation or statistical mechanical proton population of a given H^+-binding site; Q_j(pH) $= (1 - \langle s_j \rangle)$ and Q_j(pH) $= -\langle s_j \rangle$, for basic and acidic groups, respectively, where

$$\langle s_j \rangle = 10^{(\text{pH}-pK_j)}/[1 + 10^{(\text{pH}-pK_j)}] \quad (2)$$

Thus, using partial titration of each jth group, it is possible to find the pH-dependent net charge of the whole molecule, Z(pH), i.e., potentiometric titration curve

$$Z(\text{pH}) = \sum_j Q_j(\text{pH}) \quad (3)$$

W_{ij} is an empirically determined potential function for pairwise interactions (see also eq 5). r_{ij} is the distance between charged groups i and j and

$$W_{ij}(r, a_k) = \sum_k (a_k/r_{ij}^k) \quad (4)$$

$k = 1$ for long range (Columbic) interactions, $k = 2$ for midrange, charge−dipole interactions, and $k = 3$ for short-range dipole−dipole interactions. The a_k values were estimated by a nonlinear procedure (25) and were found to be relatively constant for different test sets of globular proteins by others (16−19). The above mean-field approach has been successfully applied to a variety of globular proteins and is in good agreement with the method of screened Columbic potential approximation (26, 27). Finally, SA_{ij} is the normalized averaged static solvent accessibility of the group/atom i interacting with the group/atom j (28).

The electrostatic free-energy term ΔG_{el}(pH) $\sim \Sigma \Delta pK_i$(pH) is the change in the intrinsic ionization constant pK_a of the ith site ($pK_{int,i}$) as described below: the pK_a for the ith group [pK_i(pH)] is calculated iteratively by eq 5

$$pK_i(\text{pH}) = pK(m)_i + \Delta pK(\text{sol})_i + \Delta pK(\text{per})_i + \\ \Delta pK(\text{tit})_i(\text{pH}) \quad (5)$$

where $pK(m)_i$ is the pK_a of the ith site according to model compounds (17, 21, 25, 29); $\Delta pK(\text{sol})_i$ is the Born self-energy of the ith site buried within the "uncharged" protein, and $\Delta pK(\text{per})_i$ is the contribution of the ith site interacting with the set (j) of (permanent, fixed) partial atomic charges. The term $pK(\text{tit})_i$ is the pK_a shift of the ith site caused by the interactions with all other proton-binding groups and is evaluated as reported previously (16).

If the first three pH-independent terms of eq 5 are collected under the term $pK_{int,i}$, then

$$pK_i(\text{pH}) = pK_{int,i} + \\ (1/2.3RT)\sum_{j\neq i}[Q_j(\text{pH})(W_{ij} - C)(1 - SA_{ij})] \quad (6)$$

where C is the Debye−Hückel term for ionic strength.

The atomic coordinates were mapped onto a 65 × 65 × 65 Å three-dimensional grid to obtain $\Phi_{el,i}$ (pH). An additional calculation was also performed for comparison via DELPHI at an ionic strength of 0.1 M with values for the dielectric constants assigned as 4−10 and 80 for protein and water, respectively. The results were essentially in agreement with those presented here at pH 6.5.

The 3D distribution of the EPs Φ_{el} (3D EP) was calculated at a selected pH, ionic strength, and Stern radii. These were visualized as van der Waals atomic surface potentials in a semiquantitative color scheme (blue, positive; green, neutral; and red, negative) using RasMol and extracted as GIF files. The space-distributed EP was used for correct determination of the molecular electric moment (μ_e) at a chosen pH. The electric moment of a molecule means a dipole moment (μ_d) when the pH = pI (at $Z = 0$). It is calculated as a vector from integration in the separate positive and negative centers of mass $Q^+(x,y,z)$, $Q^-(x,y,z)$ of EPs within the highly resolved 3D grid. It is possible to calculate this electric moment, which depends upon the complex dielectric environment, by the
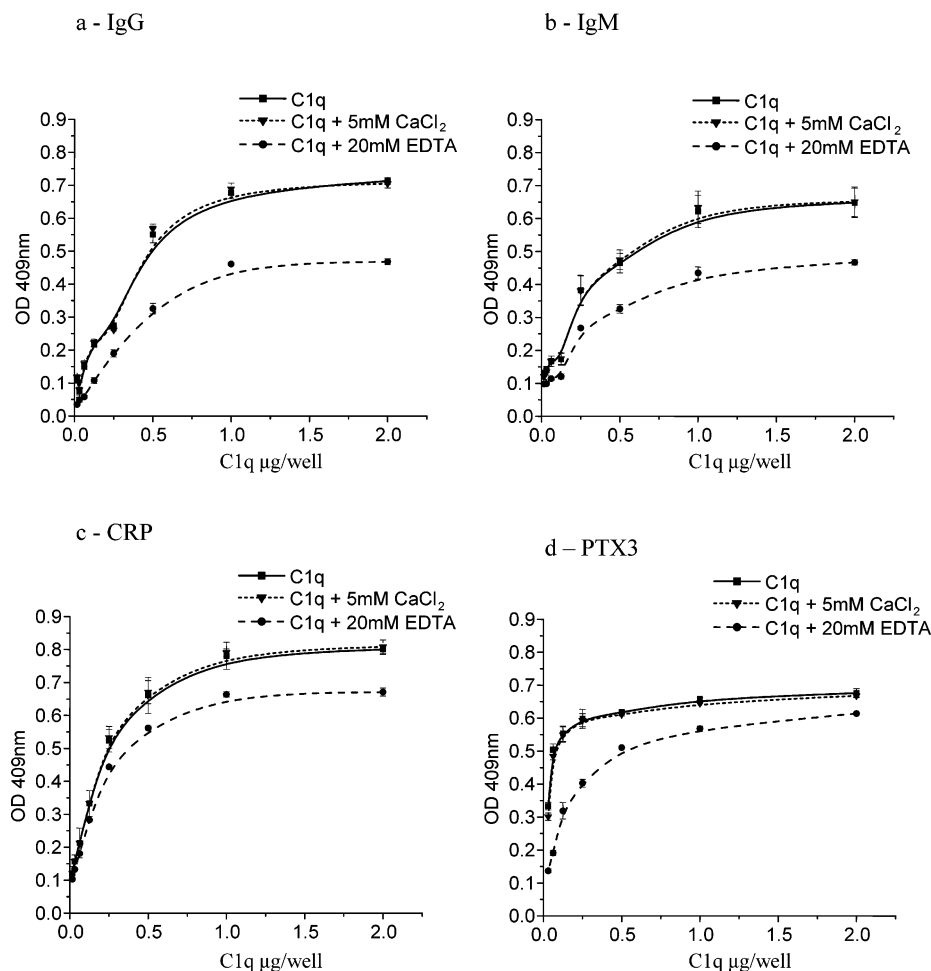
a - IgG

b - IgM

c - CRP

d – PTX3

FIGURE 1: ELISA to examine the effect of Ca^{2+} on the interaction between C1q and its targets: (a) IgG1, (b) IgM, (c) CRP, and (d) PTX3. A total of 2 μg/well heat-aggregated IgG1 or IgM or 1 μg/well CRP or PTX3 were coated on the microtiter wells for 1 h at 37 °C. After blocking with PBS containing 1% (w/v) BSA and subsequent washing, the wells were incubated with a serial dilution of C1q (from 0.0625 to 2 μg/well) in TTBS, TTBS and 5 mM $CaCl_2$, or TTBS and 20 mM EDTA overnight at 4 °C. The bound C1q was detected by rabbit anti-human C1q antibodies and anti-rabbit IgG, conjugated with AP. The data shown are the mean $\pm$ SD of triplicate measurements.

3D EP (3D Φ_{el}) of a dense grid ($d = 1$ Å, where d is the grid step). Such grids at the corresponding pI values and at pH 7.4 of the apo and holo forms were calculated, and the corresponding dipole and electric moments as well as the EP of each atom were visualized via RasMol (depicted as a dot surface of van der Waals spheres). We consider that such macroscopic electric moments are crucial in molecular recognition, as shown previously (30, 31).

RESULTS

Experimental Results: Effect of Ca^{2+} on the Interactions of C1q, ghA, ghB, or ghC with IgG1, IgM, CRP, or PTX3. We determined the amount of calcium ions bound to each recombinant globular fragment in solution by atomic absorption spectroscopy. The total calcium in the ghA solution was found to be 0.6 μg/mg of protein. This corresponds to about 1 mol of calcium ions/1 mol of ghA. For the ghB, the amount of calcium was higher, 2.6 μg/mg of protein, corresponding to about 4 mol of Ca^{2+}/1 mol of ghB. The presence of calcium was also detected in the ghC solution, which was found to be 0.2 μg/mg of protein or less than half a mole of Ca^{2+}/mol of ghC.

The interaction between C1q and the target molecules was performed with and without an excess of Ca^{2+}. The removal of Ca^{2+} from the incubation mixture was achieved by

addition of EDTA. The C1q binding to the target was reduced by about 30% for IgG1, 28% for IgM, 15% for CRP, and 10% for PTX3 in the presence of 20 mM EDTA (Figure 1). Similarly, the binding activity of the ghB module decreased by about 30% for IgG1 and 15% for IgM, CRP, as well as PTX3 in the absence of Ca^{2+} (20 mM EDTA, Figure 2). The binding of ghA to the various target molecules was only slightly altered. It was reduced to less than 10% for IgG1 and CRP. The removal of Ca^{2+}, however, had no effect on the binding of ghA to IgM as well as PTX3. No difference in the target-binding activity of ghC was found toward all four tested targets following addition of EDTA (data not shown).

To further examine the role of Ca^{2+} in the interactions between C1q, ghA, ghB, or ghC and the target molecules, a pH-scanning experiment was carried out with and without EDTA. The binding of C1q, ghA, ghB, or ghC to the target molecules was weaker in the absence of Ca^{2+} (as shown for ghB in Figure 3a). There was no significant difference in the curve characteristics for each tested target (parts a and b of Figure 3).

Theoretical Results: Z(pH) Curves. The net-charge (Z) pH dependence of the individual chains, the AB, AC, and BC chain pairs, and the ABC trimer was calculated in the presence (the holo form) or the absence (the apo form) of
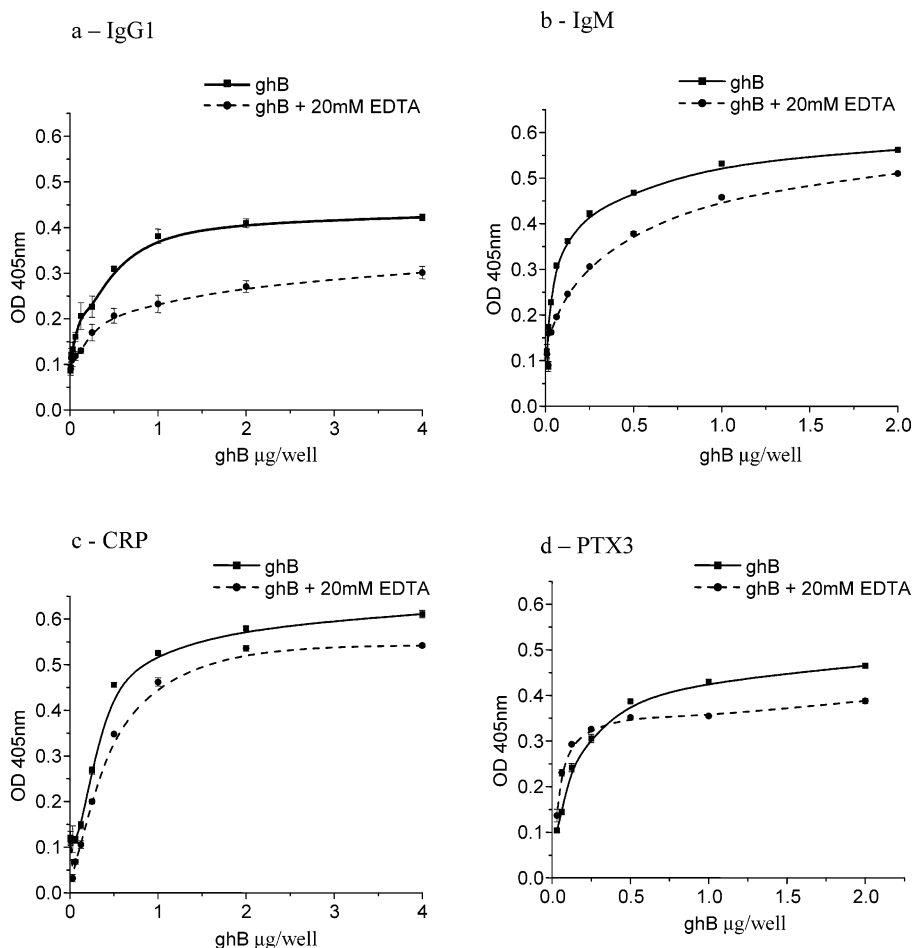
FIGURE 2: ELISA for the detection of the interaction between the ghB module and C1q targets with and without Ca^{2+}: (a) IgG1, (b) IgM, (c) CRP, or (d) PTX3. A total of 2 μg/well heat-aggregated IgG1 or IgM or 1 μg/well CRP or PTX3 were coated on the microtiter wells for 1 h at 37 °C. After blocking the wells with PBS containing 1% (w/v) BSA and subsequent washing, the wells were incubated with a serial dilution of the ghB protein (from 0.0625 to 4 μg/well) in TTBS or TTBS and 20 mM EDTA overnight at 4 °C. The bound ghB was probed using mouse anti-MBP antibodies, followed by the addition of rabbit anti-mouse IgG–HRP conjugate. The data shown are the mean ± SD of triplicate measurements.

Ca^{2+} (Figure 4a). Z(pH) curves show smaller slopes $\beta = \partial Z/\partial pH$ in the acidic region of pH than in the alkaline one. Thus, the presence of any ions in the solution will have a low impact during experimental determination of isoelectric point (pI) values. The pI value of the gC1q heterotrimer was calculated to be 9.07 (with Ca^{2+}) and 8.95 (without Ca^{2+}). Both the A and C chains had almost identical pI values of 8.8 (with Ca^{2+}) and 8.6 (without Ca^{2+}). The pI value of the B chain showed a considerable difference, being 10.2 in the holo and 9.7 in the apo forms. Notably, the net positive charge of the gC1q domain persists widely around the physiological pH 7.4, and this even increases because of the binding of Ca^{2+}. This binding shifts up all curves Z(pH) from the axis $Z = 0$, as shown in Figure 4a. An increased Z increases the reliability of the pI determinations. Subtracting the apo curves from corresponding holo curves yields the effect of Ca^{2+} on the net charge (Figure 4b). From its pH dependence, one can determine the type of ionic groups that are influenced by Ca^{2+} binding. The acidic residues in the Ca^{2+}-binding site and its surroundings appear to be most perturbed.

ΔG_{el}(pH) Curves. The comparative pH-dependent electrostatic stability of the various forms of C1q is shown in Figure 5. Theoretically estimated pH denaturation points [at ΔG_{el}(pH) = 0] in the acidic region are $pH_{d,a} = 2.9$ for both

apo and holo forms, whereas in the alkaline region $pH_{d,b}$ are 11.1 and 11.8 for them, respectively. The difference $\Delta pH_{d,b} = 0.7$ is due to the pH-independent part (i.e., hydrophobic and/or van der Waals interactions) of the free energy of the Ca^{2+} binding. The gC1q heterotrimer, monomers (A, B, and C), and the chain pairs (AB, AC, and BC) show negative values of ΔG_{el} in a broad pH range (4.5−9). The flatness of the curves for all C1q forms in the neutral pH region is remarkably similar for the apo and holo forms. The values of the maximal negative electrostatic free-energy change differed in the holo and apo forms. Only the minimal ΔG_{el} of the isolated, single globular domain of the C chain remained unchanged in both cases: −5.6 and −5.7 kcal/mol. For the minimal ΔG_{el} of the isolated, single globular domain of the A and B chains, a significant difference was observed: −4.6 and −9 kcal/mol for the holo forms and −3.8 and −4.2 for the apo forms, respectively. The order of the electrostatic stability of the globular head pairs was also changed in the presence of Ca^{2+} in comparison to when Ca^{2+} was absent: ΔG_{el}(AC) < ΔG_{el}(AB) < ΔG_{el}(BC) for the holo forms, whereas ΔG_{el}(AB) < ΔG_{el}(AC) < ΔG_{el}(BC) for the apo forms. The maximum stability (minimum ΔG_{el}) of the monomers, chain pairs, and the heterotrimer was achieved at different pH values. Furthermore, for the B chain, B-chain-bearing chain pairs, and the heterotrimer, a characteristic
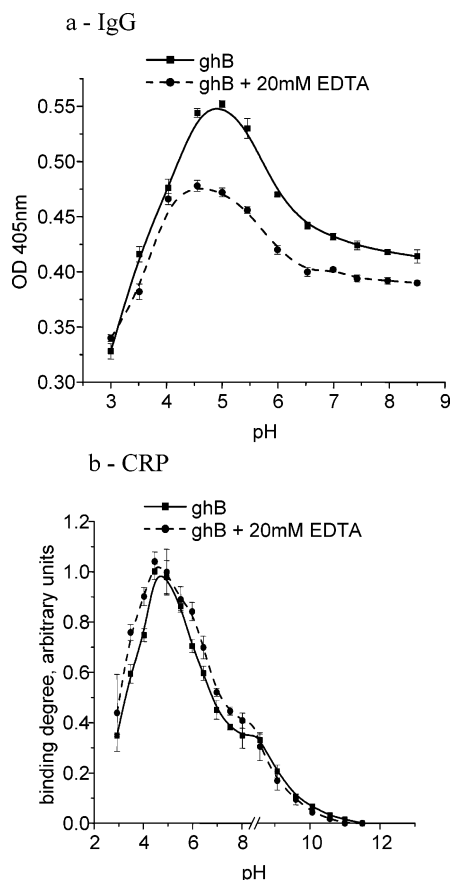
a - IgG

b - CRP

FIGURE 3: pH dependence of the interaction between the ghB and IgG or CRP with and without Ca^{2+}. (a) IgG1; (b) CRP. A total of 2 μg/well heat-aggregated IgG1 or 1 μg/well CRP was coated on the microtiter wells for 1 h at 37 °C. After blocking with PBS containing 1% (w/v) BSA and subsequent washing, the wells were incubated with 1 μg/well ghB in the assay buffer at different pH values. The bound ghB was probed using mouse anti-MBP antibodies, followed by rabbit anti-mouse IgG−HRP conjugate. The data shown are the mean ± SD of triplicate measurements. The result is presented in optical density units, measured from pH-scanning ELISA (a), or in arbitrary units (b), where the minimal observed binding was considered 0 and the maximal was considered 1.

decrease in the electrostatic free energy in the alkaline (8.5−9.5) pH region was observed. This was strengthened in the presence of Ca^{2+}, indicating that the Ca^{2+}-bound form of the protein is more stable in an alkaline environment.

Numerical evaluation of the changes of ΔG_{el} upon Ca^{2+} binding is given in Tables 1 and 2. ΔG_{el} was calculated at pH 6.5 ± 0.4. In this range, the stability of the gC1q heterotrimer was pH-independent (Table 1). Ca^{2+} weakly stabilizes the trimer ($\Delta G_{el} = -5.2$ kcal/mol), the monomers, and the chain pairs but destabilizes the interaction between the monomers and the chain pairs within the trimer. The interaction between the AC chain pair and the B chain was energetically not favorable with a reduction in stability after removal of the Ca^{2+} ion (Table 2). The weaker effect (but also diminishing interchain interactions) is observed in the case of the trimer as a sum of monomers. The binding of the A and B chains to the other chain pair is small and negative. The difference between ΔG_{holo} and ΔG_{apo} for the trimer ($\Delta\Delta G^{Ca}$) indicates the free energy of Ca^{2+} binding and can be related to the Ca^{2+}-binding association constant $K_a(Ca^{2+})$ using a classical $\Delta\Delta G^{Ca} = -RT \ln K_a(Ca^{2+})$, as well as the corresponding dissociation constant $K_d(Ca^{2+}) =$

a

b
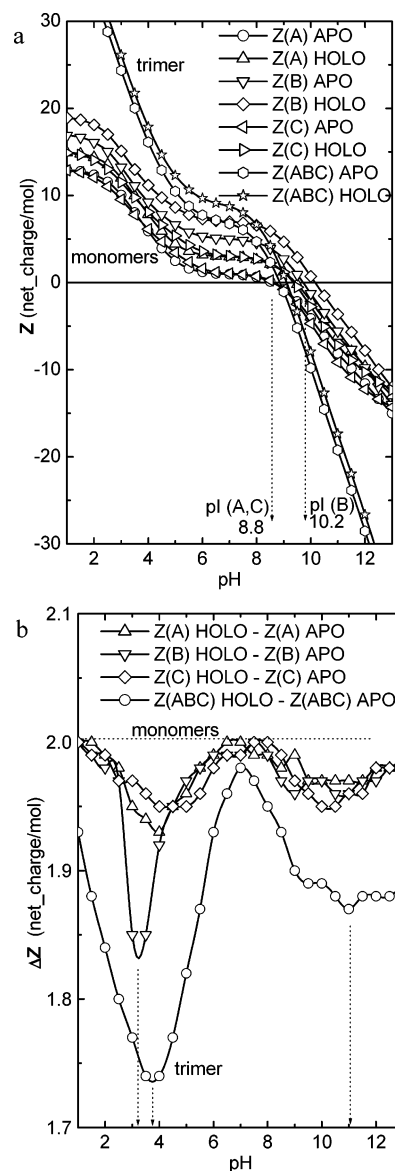
FIGURE 4: Calculated pH-dependent H^+ binding to the apo and holo forms of the C1q heterotrimer and the monomeric chains based on the crystal structure (*5*; PDB 1PK6). The results were obtained using PHEI software. (a) Theoretically predicted potentiometric titration Z (pH) curves for both forms are shown. These have isoelectric points (pI values), i.e., the pH values at which $Z = 0$, within the interval 8.8−10.8. (b) Influence of Ca^{2+} on pH-dependent H^+ binding as followed from the differences between the holo and the apo forms for each monomer and chain pair. The effect is not additive (A + B + C $\neq$ ABC) and is mostly manifested in the acidic pH region (pH 3−4) because of the interaction of Ca^{2+} with carboxylic groups.

K_a^{-1}. The overall stabilization effect of −5.2 kcal/mol for Ca^{2+} binding to the ABC trimer leads to an expected $pK_{Ca}^{2+} = 3.77$. These values correspond to low-affinity constants and can be explained by a predominantly positive charge system at pH 7.4. At pH values between 6 and 8.5, the predicted affinity of the gC1q trimer for Ca^{2+} remains almost unaltered. For the ghB module, the predicted affinity is pH-independent in the range of 5−8.5. At pH lower than 6 (for gC1q) or 5 (for the B chain), the affinity decreases dramatically.

On the basis of the crystal structure of the gC1q domain, it appears that the C chain is not involved in Ca^{2+} binding (*5*). The data presented in Table 1 indicate that Ca^{2+} mostly
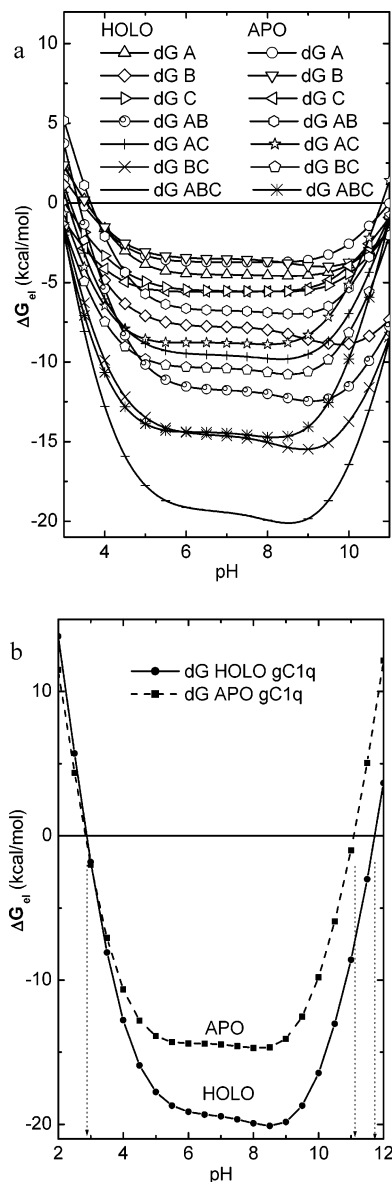
FIGURE 5: Theoretical analysis of the pH-dependent electrostatic term of free energies [ΔG_{el} (pH)], i.e., charge-dependent characteristics of the individual chains and the heterotrimeric gC1q domain. The results were obtained using PHEI software. (a) The ΔG_{el} (pH) of the A, B, and C chains (simulated monomers), the AB, AC, and BC pairs (virtual chain pairs), and the intact ABC heterotrimer are shown. These structures were derived from the X-ray crystal structure PDB 1PK6 (*5*). (b) Comparison of the pH-dependent electrostatic term of the apo and holo forms of the gC1q trimer, as shown in a but in greater detail.

Table 1: Electrostatic Free Energy in the Presence (Holo) and Absence (Apo) of Ca^{2+}

		$\Delta G_{el,i}$ (kcal/mol) at pH 6.5 $\pm$ 0.4		
		state		
type	chain	holo	apo	holo−apo
monomers	A	−4.6	−3.8	−0.8
	B	−5.6	−4.2	−1.4
	C	−8.9	−5.7	−3.2
chain pairs	AB	−9.8	−7.1	−2.7
	AC	−12.4	−8.9	−3.5
	BC	−15.5	−11.0	−4.5
trimer	ABC	−20.1	−14.9	−5.2

not affect the positive EP of the gC1q trimer at pH 7.4.

Dipole and Electric Moments of the gC1q Domain. The dipole and electric moments of the gC1q trimer and the monomeric chains represent the macroscopic result of the overall molecular EP at a given pH (7.4 in this case) and at individual pI values (Table 3). The pI values of all C1q derivatives are in the alkaline region as calculated from Z(pH) (Table 3). The averaged dipole moment for all of the protein forms (without the apo form of the monomeric C chain) is $\langle \mu_d \rangle = 58 \pm 10$ D (e Å) and can be considered small compared to other proteins (*33*). However, for the apo form of the C chain, it is only 9 D, i.e., about 7 times smaller than the rest. Because, at physiological pH, the protein net charge of the C1q derivatives increases by 1−6 positive units for the apo and 3−8 positive units for the holo forms (*19, 21, 31*), the electric moments at this pH increased to $\langle \mu_e \rangle = $ 160−460 e Å units, i.e., 3−7 times. The B chain shows high values of μ_e (288 and 401 e Å for its apo and holo forms, respectively). Furthermore, its influence on the ABC trimer electric moment at this pH is decisive; the values are 346 and 463 e Å for the apo and holo forms, respectively. This effective molecular electrical moment is a combination between positive charge excess with a given center of mass and the given dipole moment, both acting simultaneously. It is possible to calculate this electric moment, which depends upon the complex dielectric environment by the 3D EP (3D Φ_{el}) of a dense grid ($d = 1$ Å).

The moment directions undergo dramatic changes during the transformation of the apo to holo forms, which are specific for each of the isolated chains and the trimer. The negative end of the vector in both cases is close to the center of mass of the heterotrimer. As shown in Figure 7a, in the apo case, the positive end of the vector is normal to the figure plane and passes through to the solvent surface of the B chain. Introducing a Ca^{2+} ion in the holo form strongly changes the orientation of the electric moment, directing it toward the apex of the trimer (Figure 7a). The apo vector has a positive end to the molecular surface (the apo plane) with the following positively charged residues: Arg[B108], Arg[B109], Arg[B114], Arg[B129], Lys[B132], Lys[B136], and Arg[B163]. This surface also contains His[B117], Glu[B127], and Glu[B162] (Figure 7b). When the Ca^{2+} is included, the negative end near the center of mass of the trimer remains unchanged in the holo form but the positive end twists at 67.8° to the quasi-C_{3v} molecular axis and approaches the B apex (the holo plane) with positively charged residues: Lys[A173], Arg[B108], Arg[B109], Arg[B150], and Lys[C170], as well as Trp[A147], Glu[A209], Tyr[B175], Asn[B176], Asp[B201], and Asp[B104] (Figure 7c). Thus, the B chain has a dominant role in directing the dipole moment, which

stabilizes this nonbonded C chain ($\Delta\Delta G^{Ca} = -3.2$ kcal/mol, instead of −1.4 or −0.8 kcal/mol for A and B chains). This also allowed modeling of the mode of interaction of Ca^{2+} with the C chain within the trimer.

Molecular EP. The molecular EP (Φ_{el}) distribution was calculated at various pH values (ranging between 4 and 10). At the physiological pH of 7.4, the gC1q trimer in its holo form (Figure 6) is predominantly positive (colored in blue). Only part of the C chain has a negative EP near the apex. All three chains have increased negative potentials near the CLR. The contact surfaces between the A, B, and C chains (counterclockwise from top to left) apparently lack electrostatic complementarities because all of the contact areas have strong positive Φ_{el} (Figure 6). Removal of the Ca^{2+} does

Table 2: Effect of Ca^{2+}-Binding on the Electrostatic Free Energy of Monomers, Chain Pairs, and the Trimer

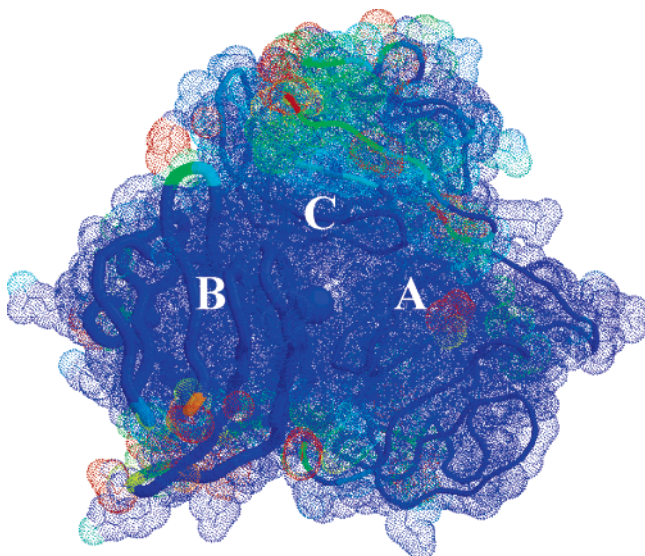| equation	state		Ca^{2+}-binding effect, (holo−apo)$\Delta\Delta G^{Ca}$ (kcal/mol) at pH 6.5 ± 0.4
	holo $\Delta\delta G$ (kcal/mol)	apo $\Delta\delta G$ (kcal/mol)	
$\Delta\delta G(AB + C) = \Delta G(ABC) - \Delta G(AB + C)$	−1.4	−2.1	+0.7
$\Delta\delta G(AC + B) = \Delta G(ABC) - \Delta G(AC + B)$	−2.1	−1.8	−0.3
$\Delta\delta G(BC + A) = \Delta G(ABC) - \Delta G(BC + A)$	0.0	−0.1	−0.1
$\Delta\delta G(T - 3M) = \Delta G(T) - [\Delta G(A) + \Delta G(B) + (C)]$	−1.0	−1.2	+0.2

FIGURE 6: EP map of the gC1q heterotrimer at pH 7.4 and ionic strength of 0.1 M e^2, obtained using PHEI software. All atomic surfaces are dotted by the colored EP (Φ_{el}) scheme: blue, positive; green, neutral; and red, negative. Ca^{2+} is colored in blue according to its charge. All three chains are mainly positive Φ_{el} (blue). A lack of charge complementarity between contacting surfaces within the trimer is also apparent.

has also been shown via the analogous analysis of the isolated chains. These data point to the participation of Arg[B108] and Arg[B109] in the positive end of the dipole moment of both the apo as well as the holo planes. It is worth noting that the surface of the holo plane is marked with a horseshoe-like area of negative EP located on the A and C chains (Figure 7d), as well as two lines of negative potential along the sides of the B chain (Figure 7b).

DISCUSSION

The human C1q has a characteristic heterotrimeric globular domain with a pseudo-3-fold symmetry (5). The crystal structure revealed modular organization of the heterotrimeric assembly, together with its different surface charge patterns and the spatial orientation of individual modules that enables the gC1q domain to interact with a diverse range of target molecules (1, 2, 5, 34). The crystal structure also confirmed the presence of a Ca^{2+}-binding site within the gC1q heterotrimer, as proposed earlier (32). Although the Ca^{2+}-binding site is located on the top of the gC1q trimer, it is not evident whether the Ca^{2+} plays a stabilizing role in the heterotrimeric assembly and/or affects the recognition properties of C1q. In the present study, we analyzed these two mutually nonexclusive possibilities using theoretical and experimental approaches.

The availability of the crystal structure of the gC1q domain of human C1q provided the basis for calculation of the electrostatic free energies and net charges of the molecule

in the presence (holo) and absence (apo) of Ca^{2+}. We also generated a full 3D map of the molecular EP for the heterotrimer. Computer simulation facilitated the division of the heterotrimer into its individual modules as monomers (A, B, and C chains) and chain pairs (AB, AC, and AB). In addition, the availability of well-characterized recombinant globular head fragments of the three chains of human C1q (ghA, ghB, and ghC) allowed an investigation of the role of Ca^{2+} on their interaction with four natural C1q-binding molecues: IgG, IgM, CRP, and PTX3, which bind C1q differentially and whose interaction with C1q is of crucial importance for the immune response. The IgG1 and CRP have defined crystal structures (31, 32), with relatively well-characterized C1q-binding sites for CRP (24, 35) and IgG1 (36). Recently, a docking model has been proposed with respect to the interaction of the gC1q domain with CRP and IgG (5). The interaction of C1q has also been examined with respect to IgM (15, 37, 38) and PTX3 (39, 40).

Differential Requirement of Ca^{2+} by C1q for Target Recognition. The atomic absorption spectroscopic experiments revealed the presence of a significant amount of calcium in the ghB sample (2.6 μg/mg), a low amount in the ghA sample (0.6 μg/mg), and a very low in the ghC sample (0.2 μg/mg). These results are consistent with the theoretical predictions and the observed decrease in the binding to the targets after Ca^{2+} removal. The most significant decrease in the ability of the monomer to bind target molecules in the absence of Ca^{2+} was evident in the case of the ghB module, which was similar to C1q (gC1q trimer). This confirms a major role of the B chain in binding Ca^{2+}. As expected, no difference in IgG1, IgM, CRP, and PTX3 binding was observed in the presence or absence of Ca^{2+} for ghC, although its binging to all targets was significant and dose-dependent. Therefore, the requirement of Ca^{2+} for the interaction of C1q with the target is different for the gC1q heterotrimer as well as the individual gC1q modules (ghA, ghB, and ghC) and specific for each tested target molecule. PTX3 seems to be the least sensitive to the presence of Ca^{2+}.

The role of Ca^{2+} on the functional activity of C1q has been investigated earlier by Paul et al. (42) who used hydrogen-exchange, differential, and CD spectroscopy to show that the presence of 5 mM CaCl$_2$ had no detectable effect on the C1q conformation. Our data also indicate that addition of an excess of CaCl$_2$ to the buffer does not alter C1q binding to its target structures. It appears that Ca^{2+} binding is an intrinsic property of the C1q molecule, and additional Ca^{2+} ions fail to influence an already occupied Ca^{2+}-binding site. Under the experimental conditions used by Paul et al. (42), neither spectroscopic nor hydrogen-exchange studies were performed in the presence of EDTA. Therefore, there is no evidence to suggest that a change in the conformation of the gC1q domain could be due to Ca^{2+} removal.

Table 3: C1q Electric (μ_e at pH 7.4) and Dipole (μ_d at pI) Moments of the Monomers (A, B, and C) and the Trimer (ABC) in the Apo (without Ca^{2+}) and Holo (with Ca^{2+}) Forms

forms			electric moments (μ_e) at pH 7.4			dipole moments (μ_d) at pI		
type	chain	state	$\langle Z \rangle$ (e)	distance (Å)	electric moment (e Å)	pI/ΔG_{el} (kcal/mol)	distance (Å)	dipole moment (e Å)
monomers	A	apo	+0.88	6.04	92	8.75/−3.7	5.72	59
		holo	+2.87	4.97	192	9.25/−4.5	4.24	61
	B	apo	+4.86	2.32	288	9.75/−3.5	4.52	57
		holo	+6.86	2.39	401	10.25/−7.8	3.26	46
	C	apo	+0.93	0.88	44	8.75/−5.6	1.06	9
		holo	+2.93	5.08	163	9.25/−5.5	4.27	59
trimer	ABC	apo	+6.06	0.83	346	8.75/−14.5	1.04	58
		holo	+8.03	1.40	463	9.25/−19.5	1.72	68

One possible reason for diminished target binding after Ca^{2+} removal is alteration in the charge characteristics of the system. To investigate this, the potentiometric titration curves [Z(pH)] were predicted for all of the monomers, AB, AC, and BC chain pairs, and the intact heterotrimer. They represent the binding of protons to protein ionic groups, which is fundamentally reflected by the pH dependence of net charges (Z). The fact that the isoelectric points are at high pH values with relatively high slopes ($\beta = \partial Z/\partial pH$) allows a more correct evaluation of the pI values. They correlate with the pI determined for the entire native C1q (pI = 10.3) (*41*). The observed difference between the experimentally obtained value for the native C1q and the one calculated for the gC1q (about 1 pH unit lower) is due to the presence of the CLR in the native form. CLR thus influences the overall pI of the native molecule. Both values are in the alkaline region; thus, gC1q is positively charged at physiological pH.

Stability of the gC1q Heterotrimer over a Broad pH Range. The influence of Ca^{2+} on the electrostatic stabilization of C1q is weak, reaching only up to −5 kcal/mol for the trimer. The apo form destabilizes the interaction between the chain pairs and the monomers. It is expected that the asymmetrical binding of an ion to a heterotrimer will increase the difference in electrostatic stability between the three chains. However, the opposite appears to be true in the case of the A, B, and C chains that become more similar in their stability in the holo form. Increasing stability of Ca^{2+} complexes at alkaline pH (8.5−9.5) is also a characteristic feature of the C1q molecule and possibly reflects a cooperative interaction of Ca^{2+} with a number of lysine residues. These lysine residues are not involved in Ca^{2+} binding, but their pK_a depends upon the interaction with Ca^{2+}, which does not change its charge with the pH. The experimental data on the binding of C1q and the recombinant globular fragments to the tested targets (Figure 7) are consistent with a broad pH-independent stability that has been predicted theoretically. Over a broad range of pH, the binding of calcium and recombinant fragments to the tested targets was significant and dose-dependent. For all of the examined interactions in this study, the binding curve traces in the presence and absence of Ca^{2+} were almost identical. The removal of Ca^{2+} thus decreased the interaction. Similar traces in both the apo and holo forms confirm that Ca^{2+} does not influence considerably the overall charge properties of the gC1q molecule. A lack of significant conformational change induced within the gC1q domain over a broad pH range has also been reported previously (*41*). The sharp change of ΔG_{el} at a pH lower than 5 correlates with data reported by others (*42*) for a small but significant conformation transition

occurring at pH 6 and a stabilization of the conformation between pH 6 and 8.

C1q recognizes some of its target molecules in the neutral pH region (about pH 7.4) or in the acidic conditions found at the sites of inflammation. This pH is shifted 3 or more pH units down the pI values. Thus, under physiological conditions, C1q has Z > 0; i.e., the molecules (trimers and monomers) are positively charged. This dominates the overall EP over a wide pH range and probably explains the repulsive interaction between the A, B, and C chains. The enhanced binding of C1q with IgG as well as CRP under mild acidic conditions (*43, 44*, this paper) probably hints at an *in vivo* mechanism for strong complement activation only under conditions of inflammation, where the pH is lowered (danger signal). A decrease in pH (pH < 6 for the gC1q domain or pH < 5 for the ghB module) probably leads to a loss of Ca^{2+} and hence a reduction in the target binding. Therefore, at a lower pH (as is the case at sites of inflammation), the binding of C1q to some of its targets (and subsequent complement activation) is under pH and Ca^{2+} control. This is of pathophysiological relevance because uncontrolled C1q interaction with its targets and subsequent activation of the classical complement pathway could lead to tissue damage and possible autoimmune manifestations. Interestingly, C1q seems to be stable over a broad pH range in the holo form, and the pH range of stability remains unaltered when Ca^{2+} is removed. The similarity in the flatness of curves in the neutral pH region for the apo and holo forms is remarkable (Figure 5).

Stabilization of Ca^{2+} within the gC1q Heterotrimer. Another interesting point that the present study highlights is that the strongest Ca^{2+} stabilization is observed for the BC chain pairs rather than the AB, which bear the ion-binding site. The interaction of a C chain with the AB chain pair is repulsive at pH 6.5 ± 0.4, with ΔG_{el} = +0.7 kcal/mol. Individual C chain and C-chain-bearing pairs are stabilized in the presence of Ca^{2+}. This suggests that the C chain (which does not have Ca^{2+}-binding amino acid residues) also senses the influence of Ca^{2+} both as a monomer and as a chain pair. Two possible mechanisms could explain this observation. First, Ca^{2+} exerts influence through the space charge effect directly to the C chain. Second, Ca^{2+} exerts a direct effect on the A and B chains. Certain charged groups within these C1q regions, which closely interact with the C chain groups, change their pK_a values when Ca^{2+} is removed, thus destabilizing the interchain interactions. We consider the latter more likely.

Inherent Electrostatic Instability of the gC1q Heterotrimer. When the electrostatic stability of the gC1q trimer was compared with a sum of the stabilities of the isolated

FIGURE 7: Electric moment direction in the gC1q trimer (pH 7.4, ionic strength = 0.1). The red circle indicates the negative end of the vector, which is in the same position in both apo and holo images. The yellow circle is the calcium ion, and the small blue circle represents where the calcium ion would be in the case of the apo form. The space-distributed EP was used for the determination of the molecular electric moment at the chosen pH. The molecular electric moment was calculated as a vector from the integration at the separate positive and negative centers of mass $Q^+(x,y,z)$, $Q^-(x,y,z)$. (a) Electric moment (μ_e) vectors for the holo (light blue) and apo (dark blue) forms are calculated at pH 7.4 and an ionic strength of 0.1. The polypeptide chain trace is 2.5 times thicker for the B chain than for the A or C chains. The coloring is meant to represent EP, blue for positive and red for negative. Dashed lines represent the planes approximately perpendicular to the μ_e vectors and the figure plane. The dotted line passes through the Arg^{B109} and Asn^{B104} residues (light blue). With the adjacent Arg^{B108}, they belong to both planes. (b) Holo plane, the trace of three chains and side chains are colored by the EP scheme calculated at pH 7.4 with an ionic strength of 0.1. The figure plane and the labeled residues correspond to the molecular apex, approximately perpendicular to the molecular axis and the electric moment (μ_e) in the holo form (close to the putative CRP-binding site). The red point close to the Ca^{2+} ion (yellow) is the negative center of mass of the μ_e. The dotted line connecting Arg^{B109} and Asn^{B104}, with the adjacent Arg^{B108}, are on both the holo and apo planes. The last few residues are not shown but include those left of the dotted line. The negative EP (red colored residues) borders the central positive EP platform. (c) Apo plane, the trace of the three chains and the side chains are colored by the EP scheme calculated at pH 7.4 and an ionic strength of 0.1. The figure plane and the labeled residues correspond to the solvent-exposed surface of the B chain (close to the IgG-binding site). (d) Positive EP border with a horseshoe-like appearance. This directs the molecular turn when Ca^{2+} is removed.

monomers, a positive value for $\Delta G_{el} = +0.2$ kcal/mol was observed. The surprising finding that the individual C1q globular fragments are electrostatically preferred over the natively occurring composite heterotrimer reaffirms the existence of modularity within the gC1q domain (*1, 2, 15, 45*). This feature could be explained by the unusual fact that repulsive rather than attractive charge−charge interactions are observed between the contact surfaces of the gC1q trimer. The contact areas are not complementary with their EPs. It is clear that specific hydrophobic interactions have a defini-

tive role in giving rise to the heterotrimeric structure of the gC1q domain (*2, 5, 34*). This inherent electrostatic instability may play a role in the C1q function. Using unchanged atomic coordinates and adding Ca^{2+} at its place for each A, B, and C monomeric chain, we noticed that Ca^{2+} mostly stabilizes the nonbonded C chain (−3.2 kcal/mol compared to −1.4 for the A chain or −0.8 kcal/mol for the B chain). The presence of a negative EP on the "top" (the apex) of the C chain seems to be the most likely explanation. Ca^{2+} has a smaller stabilization effect even on the AB chain pair (−2.7

kcal/mol). Considering that the stabilization effect on the ABC trimer is −5.2 kcal/mol, it seems that the dissociation of the trimer should reduce the Ca^{2+}-binding affinity of the B chain 3 times (from −5.2 to −1.4 kcal/mol). This can be of functional importance if the macrodipole of the gC1q domain significantly changes because of Ca^{2+} binding. Moreover, the binding of the apo form of the C chain to the Ca^{2+}-bound AB chain pair is an energetically unfavorable process, and it could participate in the chain dissociation during the C1q−target interaction.

An Important Role of the Electric Moment in Target Recognition by C1q. The detailed analysis of 3D EP at pI ($Z = 0$) and at physiological pH 7.4 gave us the dipole and electric moments of all forms of C1q (Table 3). It is remarkable that the dipole moments are very small for such a big molecule: $\mu_d = 58 \pm 10$ D for most chains and forms, and $\mu_d = 9$ D only for the apo C chain. This shows a highly correlated 3D charge distribution (*17*) optimized by ionic groups and confirms an important biological role of the macroscopic dipole interactions (*30, 46*). The small dipole moment and highly correlated 3D charge distribution will not be altered significantly upon point mutation, and these could serve as a mechanism to protect the functional activity of the gC1q domain from naturally occurring mutations. An increase in the electric moment (7 times or more) is calculated when the pH is changed to the physiological value. This suggests a leading role for the electric moment in the target recognition properties of C1q. The heterotrimer electric moment at pH 7.4 was calculated to be 346 and 463 e Å for the apo and holo forms, respectively. Thus, big lobes of positive EP were found on the outside of the A and B chains. Corresponding vectors show the direction of the electrostatic field extension, which is under Ca^{2+} control. In the heterotrimeric gC1q apo form, the electric moment vector is perpendicular to the quasi-C_{3v} molecular axis. In its holo form, the vector changes direction by 87° and stands parallel to the same axis, pointing toward the apex of the molecule. The direction of the electrical moment vectors predicted for the gC1q trimer is similar to that of the monomeric B chain. This reorientation of the electric moment vector probably explains the reduction in C1q binding to the target molecules following calcium removal (i.e., after the addition of EDTA). Thus, in the planes normal to the electric moment vectors in the holo and apo forms (that are approximately perpendicular to one another; Figure 7a), the following positively charged surface residues can be found: the apo vector, Arg^{B163}, Lys^{B136}, Arg^{B129}, Arg^{B108}, Arg^{B109} Arg^{B114}, and Lys^{B132} (Figure 7b); the holo vector, Lys^{A173}, Arg^{B108}, Arg^{B109}, Arg^{B150}, and Lys^{C170} (Figure 7c).

Residues in the Holo and Apo Planes that Are Crucial for gC1q−Target Interaction. The holo plane also includes Tyr^{B175} that protrudes above the molecular surface, Asn^{B104} (neutral amino acid residue but in the area with a positive potential), Trp^{A147}, Asn^{B176}, Asp^{B201}, Glu^{A209}, as well as several other residues (Figure 7c). Interestingly, Lys^{B202} that lies between Asp^{B201} and Glu^{A209} is buried in an area of negative EP. Thus, the positive EP is focused and directed toward the left side (Figure 7d), facilitating the μ_e vector to rotate to about 90° to the left following removal of the Ca^{2+} ion. The apo plane, apart from its characteristic cluster of positively charged residues, also contains Asn^{B104} (in the positive EP), His^{B117}, Glu^{B127}, Glu^{B162}, and other residues,

as shown in Figure 7b. These residues form two surfaces, which could potentially participate in target binding. These highly variable residues within the gC1q family members have been previously predicted via ConSurf (*1*). The molecular surface associated with the electrical moment vector in the holo form is close to the proposed CRP-binding site (*1, 5*), and in case of the apo form, it is near the IgG-binding site of C1q. The contributions of Arg^{B114}, Arg^{B129}, and Arg^{B163}, as well as His^{B117}, in IgG recognition by C1q have been experimentally demonstrated (*47*), and a possible role of Tyr^{B175} and Lys^{C170} has recently been verified via mutational analysis (Roumenina et al., manuscript in preparation). The importance of Arg^{B108} and Arg^{B109} in C1q binding to fucoidan and IgG has been recently published (*48*). Thus, a number of residues belonging to the two planes (holo and apo) have been experimentally shown to be crucial for the C1q−target interaction.

Within the B chain, Arg^{B108}, Arg^{B109}, and Asn^{B104} are common in both the apo and holo planes. This suggests that the rotation probably occurs around the Arg^{B108}−Arg^{B109}−Asn^{B104} axis and that the gC1q heterotrimer can reorient itself from one plane to another upon Ca^{2+} binding without moving from this axis. Moreover, this is the only rotation possible following C1q binding to negatively charged target molecules, because the Arg^{B108}−Arg^{B109}−Asn^{B104} axis alone on the apex has a positive EP (Figure 7c). The negative potential over the A and C chains directs the molecular turn when Ca^{2+} is removed. This conformational change could initiate the mechanical stress that gets transmitted through to the C1q−C1r−C1s interface from the CLR to the C1r catalytic region when C1 binds to a target (*6*).

In conclusion, the present study supports the argument for the modularity within the gC1q domain and highlights issues relevant for the differential recognition of target molecules by C1q (*1, 4, 15*). Having confirmed a role of Ca^{2+} and the external molecular EP in the target recognition by C1q, we propose a model for the C1q−target interaction: (i) C1q in serum is present in the Ca^{2+}-bound form and its molecular electrical moment is directed toward the apex of the gC1q heterotrimer; (ii) in the initial phase of the C1q−target interaction, when bound to C1q, Ca^{2+} facilitates recognition of negatively charged molecules; (iii) the negative field of the target molecule accelerates calcium removal from C1q; (iv) this leads to mechanical stress and a structural change within the CLR domain and, hence, C1r activation; and (v) at the sites of inflammation, the C1q−target interaction is influenced by the pH and the Ca^{2+} concentration. We propose that, at least in the case of the C1q−IgG interaction, the change to the apo form causes the gC1q heterotrimer to rotate around the Arg^{B108}−Arg^{B109}−Asn^{B104} axis without breaking these ionic links to the target, leading to transmission of the activation signal to C1r.

REFERENCES

1. Kishore, U., Ghai, R., Greenhough, T. J., Shrive, A. K., Bonifati, D. M., Gadjeva, M. G., Waters, P., Kojouharova, M. S., Chakraborty, T., and Agrawal, A. (2004) Structural and functional anatomy of the globular domain of complement protein C1q, *Immunol. Lett. 95*, 113−128.

2. Kishore, U., Gaboriaud, C., Waters, P., Shrive, A. K., Greenhough, T. J., Reid, K. B. M., Sim, R. B., and Arlaud, G. J. (2004) C1q and tumor necrosis factor superfamily: Modularity and versatility, *Trends Immunol. 10*, 551−561.

3. Arlaud, G. J., Gaboriaud, C., Thielens, N. M., Rossi, V., Bersch, B., Hernandez, J. F., and Fontecilla-Camps, J. C. (2001) Structural biology of C1: Dissection of a complex molecular machinery, *Immunol. Rev. 180*, 136−145.

4. Arlaud, G. J., Gaboriaud, C., Thielens, N. M., Budayova-Spano, M., Rossi, V., and Fontecilla-Camps, J. C. (2002) Structural biology of the C1 complex of complement unveils the mechanisms of its activation and proteolytic activity, *Mol. Immunol. 39*, 383−394.

5. Gaboriaud, C., Juanhuix, J., Gruez, A., Lacroix, M., Darnault, C., Pignol, D., Verger, D., Fontecilla-Camps, J. C., and Arlaud, G. J. (2003) The crystal structure of the globular head of complement protein C1q provides a basis for its versatile recognition properties, *J. Biol. Chem. 278*, 46974−46982.

6. Gaboriaud, C., Thielens, N. M., Gregory, L. A., Rossi, V., Fontecilla-Camps, J. C., and Arlaud, G. J. (2004) Structure and activation of the C1 complex of complement: Unraveling the puzzle, *Trends Immunol. 25*, 368−373.

7. Bodmer, J. L., Schneider, P., and Tschopp, J. (2002) The molecular architecture of the TNF superfamily, *Trends Biochem. Sci. 27*, 19−26.

8. Bogin, O., Kvansakul, M., Rom, E., Singer, J., Yayon, A., and Hohenester, E. (2002) Insight into Schmid Metaphyseal Chondrodysplasia from the crystal structure of the collagen X NC1 domain trimer, *Structure 10*, 165−173.

9. Schwaller, B. (2001) Calcium-binding proteins, *Encyclopedia of Life Sciences*, Nature Publishing Group.

10. Kvansakul, M., Bogin, O., Hohenester, E., and Yayon, A. (2003) Crystal structure of the collagen α1 (VIII) NC1 trimer, *Matrix Biol. 22,* 145−152.

11. Shapiro, L., and Scherer, P. E. (1998) The crystal structure of a complement-1q family protein suggests an evolutionary link to tumor necrosis factor, *Curr. Biol. 8*, 335−338.

12. Stoiber, H., Ebenbichler, C. F., Thielens, N. M., Arlaud, G. J., and Dierich, M. P. (1995) HIV-1 rsgp41 depends on calcium for binding of human C1q but not for binding of gp120, *Mol. Immunol. 32*, 371−374.

13. Sjoberg, A., Onnerfjord, P., Morgelin, M., Heinegard, D., and Blom, A. M. (2005) The extracellular matrix and inflammation. Fibromodulin activates the classical pathway of complement by directly binding C1q, *J. Biol. Chem. 280*, 32301−32308.

14. Reid, K. B. M. (1982) C1q, *Methods Enzymol. 82* (part A), 319−324.

15. Kishore, U., Gupta, S. K., Perdikoulis, M. V., Kojouharova, M. S., Urban, B. C., and Reid, K. B. M. (2003) Modular organization of the carboxyl-terminal, globular head region of human C1q A, B, and C chains, *J. Immunol. 171*, 812−820.

16. Karshikoff, A. (1995) A simple algorithm for calculation of multiple site titration curves, *Protein Eng. 8*, 243−248.

17. Spassov, V. Z., Karshikov, A. D., and Atanasov, B. P. (1989) Electrostatic interactions in proteins: A theoretical analysis of lysozyme ionization, *Biochim. Biophys. Acta 999*, 1−6.

18. Miteva, M. A., Kossekova, G. P., Villoutreix, B. O., and Atanasov, B. P. (1997) Local electrostatic potentials in pyridoxal phosphate labelled horse heart cytochrome *c*, *J. Photochem. Photobiol. 37*, 74−83.

19. Atanasov, B. P., Mustafi, D., and Makinen, M. W. (2000) Protonation of the β-lactam nitrogen is the trigger event in the catalytic action of class A β-lactamases, *Proc. Natl. Acad. Sci. U.S.A. 97*, 3160−3165.

20. Gilson, M., Sharp, K., and Honig, B. (1988) Calculating the electrostatic potential of molecules in solution: Method and error assessment, *J. Comput. Chem. 9*, 327−335.

21. Sharp, K. A., and Honig, B. (1990) Electrostatic interactions in macromolecules: Theory and applications, *Annu. Rev. Biophys. Chem. 19*, 301−332.

22. Weiner, S., Kollman, P. A., Case, D. A., Singh, U. C., Ghio, C., Alagona, G., Profeta, J. S., and Weiner, P. (1984) A semi-empirical force-field of AMBER, *J. Am. Chem. Soc. 106*, 765−784.

23. Westbrook, J., Feng, Z., Chen, L., Yang, H., and Berman, H. M. (2003) The Protein Data Bank and structural genomics, *Nucleic Acid Res. 31*, 489−491.

24. Agrawal, A., Shrive, A. K., Greenhough, T. J., and Volanakis, J. E. (2001) Topology and structure of the C1q-binding site on C-reactive protein, *J. Immunol. 166*, 3998−4004.

25. Karshikov, A. D., Engh, R., Bode, W., and Atanasov, B. P. (1989) Electrostatic interactions in proteins: calculation of the electrostatic term of free energy and the electrostatic potential field, *Eur. Biophys. J. 17*, 287−297.

26. Mehler, E. L. (1996) A self-consistent, free energy based approximation to calculate pH dependent electrostatic effects in proteins, *J. Phys. Chem. 67*, 2728−2739.

27. Mehler, E. L., and Guarnieri, F. (1999) A self-consistent, microenvironment modulates screened coulomb potential approximation to calculate pH-dependent electrostatic effects in proteins, *Biophys. J. 75*, 3−22.

28. Lee, B., and Richards, F. M. (1971) The interpretation of protein structures: Estimation of static accessibility, *J. Mol. Biol. 55*, 379−400.

29. Honig, B., Sharp, K., and Gilson, M. (1989) Electrostatic interactions in proteins, *Prog. Clin. Biol. Res. 289*, 65−74.

30. Felder, C. F., Botti. S. A., Lifson. S., Silman, I., and Sussman, J. L. (1997) External and internal electrostatic potentials of cholinesterase models, *J. Mol. Graphics Mod. 15*, 318−327.

31. Gilson, M. K. (1993) Multiple-site titration and molecular modeling: Two rapid methods for computing energies and forces for ionizable groups in proteins, *Proteins: Struct., Funct., Genet. 15*, 266−282.

32. Villiers, C. L., Arlaud, G. J., Painter, R. H., and Coulomb, M. G. (1980) Calcium binding properties of the C1 subcomponents C1q, C1r, and C1s, *FEBS Lett. 117*, 289−294.

33. Takashima, S. (1989) *Electrical Properties of Biopolymers and Membranes*, Adam Hilger, Bristol, Philadelphia, PA.

34. Kishore, U., Kojouharova, M. S., and Reid, K. B. M. (2002) Recent progress in the understanding of the structure−function relationships of the globular head regions of C1q, *Immunobiology 205*, 355−364.

35. Bang, R., Marnell, L., Mold, C., Stein, M. P., Du Clos, K. T., Chivington-Buck, C., and Du Clos, T. W. (2005) Analysis of binding sites in human C-reactive protein for FcγR I, FcγR IIa, and C1q by site-directed mutagenesis, *J. Biol. Chem. 280*, 25095−25102.

36. Idusogie, E. E., Presta, L. G., Gazzano-Santoro, H., Totpal, K., Wong, P. Y., Ultsch, M., Meng, Y. G., and Mulkerrin, M. G. (2000) Mapping of the C1q binding site on rituxan, a chimeric antibody with a human IgG1 Fc, *J. Immunol. 164*, 4178−4184.

37. Arya, S., Chen, F., Spycher, S., Isenman, D. E., Shulman, M. J., and Painter, R. H. (1994) Mapping of amino acid residues in the Cμ3 domain of mouse IgM important in macromolecular assembly and complement-dependent cytolysis, *J. Immunol. 152*, 1206−1212.

38. Chen, F. H., Arya, S. K., Rinfret, A., Isenman, D. E., Shulman, M. J., and Painter, R. H. (1997) Domain-switched mouse IgM/IgG2b hybrids indicate individual roles for Cμ2, Cμ3, and Cμ4 domains in the regulation of the interaction of IgM with complement C1q, *J. Immunol. 159*, 3354−3363.

39. Bottazzi, B., Vouret-Craviari, V., Bastone, A., De Gioia, L., Matteucci, C., Peri, G., Spreafico, F., Pausa, M., D'Ettorre, C., Gianazza, E., Tagliabue, A., Salmona, M., Tedesco, F., Introna, M., and Mantovani, A. (1997) Multimer formation and ligand recognition by the long pentraxin PTX3. Similarities and differences with the short pentraxins C-reactive protein and serum amyloid P component, *J. Biol. Chem. 272*, 32817−32823.

40. Nauta, A. J., Bottazzi, B., Mantovani, A., Salvatori, G., Kishore, U., Schwaeble, W. J., Gingras, A. R., Tzima, S., Vivanco, F., Egido, J., Tijsma, O., Hack, E. C., Daha, M. R., and Roos, A. (2003) Biochemical and functional characterization of the interaction between pentraxin 3 and C1q, *Eur. J. Immunol. 33*, 465–473.

41. Liberti, P. A., and Paul, S. M. (1978) Gross conformation of Clq: A subcomponent of the first component of complement, *Biochemistry 17*, 1952–1958.

42. Paul, S. M., Baillie, R. D., and Liberti, P. A. (1978) Solvent effects on the structure of rabbit Clq, a subcomponent of the first component of complement, *J. Biol. Chem. 253*, 5658–5664.

43. Wines, B. D., and Easterbrook-Smith, S. B. (1990) Carbodiimide crosslinking of human C1q and rabbit IgG, *Mol. Immunol. 27*, 221–226.

44. Miyazawa, K., and Inoue, K. (1990) Complement activation induced by human C-reactive protein in mildly acidic conditions, *J. Immunol. 145*, 650–654.

45. Kishore, U., and Reid, K. B. M. (1999) Modular organization of proteins containing a C1q-like globular domain, *Immunopharmacology 42*, 15–21.

46. Honig, B., Sharp, K. A., and Yang, A. S. (1993) Macroscopic models of aqueous solutions: Biological and chemical applications, *J. Phys. Chem. 97*, 1101.

47. Kojouharova, M. S., Gadjeva, M. G., Tsacheva, I. G., Zlatarova, A., Roumenina, L. T., Tchorbadjieva, M. I., Atanasov, B. P., Waters, P., Urban, B. C., Sim, R. B., Reid, K. B. M., and Kishore, U. (2004) Mutational analyses of the recombinant globular regions of human C1q A, B, and C chains suggest an essential role for arginine and histidine residues in the C1q-IgG interaction, *J. Immunol. 172*, 4351–4358.

48. Tissot, B., Gonnet, F., Iborra, A., Berthou, C., Thielens, N., Arlaud, G. J., and Daniel, R. (2005) Mass spectrometry analysis of the oligomeric C1q protein reveals the B chain as the target of trypsin cleavage and interaction with fucoidan, *Biochemistry 44*, 2602–2609.